European Journal of Pharmaceutics and Biopharmaceutics 221 (2026) 114989

Contents lists available at ScienceDirect

European Journal of Pharmaceutics and Biopharmaceutics

journal homepage: www.elsevier.com/locate/ejpb

A refined coadministration regime to mitigate immunological clearance of biomedical nanoparticles

Kathrin Schorr, Johannes Konrad, Jan Birringer, Carsten Damm, Miriam Breunig, Achim Goepferich *

Department of Pharmaceutical Technology, University of Regensburg, 93053 Regensburg, Bavaria, Germany

ARTICLE INFO

Keywords:
Subcutaneous administration
Effector nanoparticles
Coadministration regime
Endocytosis inhibitor
Phagocytosis suppression
Nanoparticle clearance
Biodistribution
Macrophages

ABSTRACT

Nanoparticles are frequently designed as carriers to mediate the active transport of their cargo to the site of action, thereby serving as effector particles. However, after their in vivo administration, they become quickly recognized by immune cells and are cleared from the systemic circulation. This significantly impairs the nanoparticles' targeting efficiency and shifts the target/off-target ratio toward metabolizing organs. As engineering-driven strategies, such as the PEGylation of their surface, require major modifications of the nanoparticles' structure and do not appear to achieve the desired level of effectiveness, synergistic approaches are attracting increasing attention. They rely on the transient blockade of the immune system through endocytosis inhibitors or decoy nanomaterials. In the present study, we introduce a further development of these synergistic approaches by loading lipid nanocapsules (LNCs) as decoy nanoparticles with the endocytosis inhibitor chloroquine. Two principal advantages can be ascribed to this refined synergistic approach: First, encapsulation of the endocytosis inhibitor paves the way for pioneering subcutaneous application as a novel route of administration for the effector nanoparticles, as phagocytic cells within the lymphatic system can be selectively targeted. Second, the established co-administration regime constitutes a transferable concept across diverse settings without the need for structural modifications of the respective effector nanoparticles. Here, we report the successful in vitro establishment of this refined coadministration regime. Preincubation with chloroquine-loaded LNCs led to a statistically significant uptake inhibition of model effector nanoparticles into macrophages. Moreover, we investigated, for the first time, the incorporation of 1,2-Dioleoyl-*sn*-glycero-3-phosphoserine as a macrophage-specific targeting structure into the decoy LNCs' envelope and its effect on the phagocytosis activity of macrophages.

1. Introduction

Over the past decades, the development of biomedical nanoparticles has been motivated by the presumption that they could serve as a platform technology for innovative drug delivery systems [1–3]. However, although nanoparticles exhibit notable efficiency under in vitro conditions, their respective in vivo performance falls short of expectations. A widely cited *meta*-analysis by Wilhelm et al. [4] has revealed that only 0.7 % of tumor-targeted nanoparticles successfully reached their target sites in vivo. A key limitation affecting their targeting efficiency is that, following systemic administration, 95 % of the effector nanoparticles (ENPs) are sequestered by cells of the mononuclear phagocyte system (MPS) and subsequently accumulated in off-target tissues, especially the liver [5–8]. This is attributed to their quick recognition by the immune system as foreign, pathogen-like material [9–11] and removal from the systemic circulation by phagocytic cells, e.g. macrophages [12,13]. The resulting reduced bioavailability of the ENPs dramatically affects their targeting efficiency, even after

Abbreviations: 100 %-DOPS-LNCs, LNCs, in which the DOPC is quantitatively substituted with DOPS; COOH-NPs, Polymeric core-shell nanoparticles carrying carboxy-terminated PEG-chains on their surface; DiO, DiOC 18(3); DOPC, 1,2-Dioleoyl-*sn*-glycero-3-phosphocholine; DOPS, 1,2-Dioleoyl-*sn*-glycero-3-phosphoserine; EE, Encapsulation efficiency; ENPs, Effector nanoparticles; FDA, Food and Drug Administration; LNCs, Lipid nanocapsules; MPS, Mononuclear phagocyte system; PICALM, Phosphatidylinositol binding clathrin assembly protein; PMA, Phorbol-12-myristate-13-acetate; s.c., subcutaneous.

* Corresponding author.
E-mail addresses: kathrin.schorr@ur.de (K. Schorr), johannes.konrad@ur.de (J. Konrad), jan.birringer@ur.de (J. Birringer), carsten.damm@ur.de (C. Damm), miriam.breunig@ur.de (M. Breunig), achim.goepferich@ur.de (A. Goepferich).

https://doi.org/10.1016/j.ejpb.2026.114989
Received 26 September 2025; Received in revised form 21 December 2025; Accepted 10 January 2026
Available online 18 January 2026

intravenous administration.

To address the ENPs' poor targeting efficiency in vivo, several engineering-driven approaches have been developed to optimize their design and to shield them from detection by the immune system [14–16]. A common strategy involves grafting ENPs with polyethylene glycol (PEG) [17–19] or zwitterionic polymers [20–22] to reduce the nanoparticle-induced complement activation and their opsonization. More advanced approaches include coating the surface of ENPs with cell membranes [23] and employing living cells as transport vehicles, referred to as "cell hitchhiking" [24]. Furthermore, CD47 or structurally-related synthetic peptides have been tested as ligands to mitigate the ENPs' phagocytosis [25–28]. CD47 is a "marker-of-self" in various species. It impedes phagocytosis by interacting with the signal regulator protein α, which is expressed by macrophages and dendritic cells [25,29]. Although all aforementioned approaches significantly extended the circulation half-life of nanoparticles, they have either not achieved a breakthrough success [30] or require a significant modification of the ENPs' surface with ligands. Accordingly, recent studies have introduced complementary approaches based on a modulation of the MPS system to delay or reduce the recognition of ENPs, thereby circumventing the need to engineer new ENPs [6,31]. The coadministration of several endocytosis inhibitors with ENPs has been tested to specifically suppress their phagocytosis by MPS cells [5,32]. Chloroquine, a FDA-approved antimalarial medication, is one of the lead compounds investigated as MPS modulating drug [30,33]. It reduces the expression of phosphatidylinositol binding clathrin assembly protein (PICALM) and thus interferes with the function of clathrin-mediated endocytosis [33]. Wolfram et al. [33] have shown that the uptake of intravenously applied ENPs by macrophages was significantly reduced as well as their liver and spleen accumulation, after preconditioning with chloroquine. As a drug-free alternative, coadministration regimes with large doses of non-toxic decoy agents, e.g. nanomaterials, have been tested to temporarily saturate the uptake capacity of the macrophages for the subsequently applied ENPs [34–36]. However, a synergistic approach combining ENP engineering, e.g. via PEGylation, with the complementary modulation of the immune system, using endocytosis inhibitors, appears most effective to improve the ENPs targeting efficiency [33].

A further refinement of this synergistic approach could involve the encapsulation of the endocytosis inhibitors into decoy nanomaterials. This strategy is anticipated to offer several benefits. Drug-loaded decoy nanomaterials are expected to exhibit a distribution pattern across reticuloendothelial system organs qualitatively similar to that of ENPs following intravenous administration [37]. The surface of the decoy nanoparticles could be functionalized with targeting moieties for the specific uptake into cells with phagocytic activity. This could amplify their specific effect on the MPS. Furthermore, it would allow for the implementation of subcutaneous administration routes for ENPs, which has so far rarely been pursued. The inherent challenge of applying ENPs subcutaneously is determined by the fact that their size (typically > 10 nm and ≤ 100 nm) prevents their direct uptake from the subcutaneous tissue into the systemic circulation via small blood vessels [38–40]. Instead, they must enter the blood circulation via the lymphatic system (Fig. S1) [41]. In the lymph vessels, the ENPs are quantitatively cleared by MPS cells, a process referred to as "lymphatic first-pass transit" [41]. Encapsulation of endocytosis inhibitors in decoy nanoparticles, followed by their subcutaneous co-administration with ENPs, promotes lymphatic uptake of both particle types [42]. Endocytosis inhibitor-loaded decoy nanoparticles are thus expected to attenuate ENPs' lymphatic clearance via local suppression of macrophage phagocytic activity within lymph vessels.

The aim of the present study was to contribute to a refinement of the synergistic approach by encapsulating an endocytosis-inhibitor into decoy particles and thus to enable subcutaneous coadministration regimes with ENPs. CY-5-labeled polymer core–shell nanoparticles were employed as model ENPs. They were composed of poly(D,L-lactide-co-glycolide) (PLGA) covalently coupled to cyanine-5-amine as core material and poly(ethylene glycol)-b-poly(D,L-lactide) (PLA-PEG) copolymer as an adhering shell. The surface of the ENPs is thus protected from excessive opsonization due to the grafting with PEG following an engineering-driven approach. PEG grafting onto ENPs' surfaces thus protects against excessive opsonization. Yet, the surface remains accessible to functionalization with ligands for active targeting applications [43–45]. To refine the synergistic approach of immunomodulation, chloroquine, as endocytosis inhibitor, was encapsulated into lipid nanocapsules (LNCs) as decoy particles (Fig. 1). The chloroquine-loaded LNCs were evaluated for their effect on phagocytosis inhibition in coadministration regimes with ENPs via flow cytometry experiments. Therefore, THP-1 monocytes were employed as target cell line and differentiated into macrophages. The mean fluorescence intensity associated with the macrophages was used as indicator for the uptake of the CY-5-labeled ENPs. Furthermore, the efficiency of a macrophage-specific targeting moiety localized in the envelope of the decoy LNCs was investigated. Therefore, 1,2-dioleoyl-*sn*-glycero-3-phosphoserine (DOPS), an "eat-me signal" for macrophages [46–48], was incorporated into the structure of the LNCs to promote their targeted uptake into macrophages and the effect of the engineered LNCs was critically evaluated.

2. Results

2.1. Characterization of the model effector nanoparticles

The nanoparticles chosen as model ENPs in this study were PLGA/PLA-PEG core–shell nanoparticles. They are already well established [49,50] successful drug delivery systems [51,52]. The nanoparticles were obtained by nanoprecipitation, with the hydrophobic PLGA and PLA aggregating in the nanoparticle core [53,54]. This results in hydrophilic PEG chains extending as a brush-like corona from the core. The hydrodynamic diameter of the ENPs was determined to be 78.31 ± 2.39 nm (mean ± SD from three independent batches) and the PDI to be 0.142 ± 0.028. The rigid, tethered morphology of the nanoparticles and considerations on the PEG conformation have already been described in previous studies [43,49]. Carboxy-terminated PEG chains were chosen for engineering the nanoparticle shell. The negative surface charge, reflected by their zeta potential of -29.1 ± 20.0 mV (mean ± SD from three independent batches), increases the stability of the nanoparticles in aqueous media and prevents their aggregation. PLGA was covalently labeled with cyanine-5-amine to make the nanoparticles accessible for detection in flow cytometry experiments.

2.2. Evaluation of LNCs as decoy agents and chloroquine as endocytosis inhibitor

Unmodified LNCs were evaluated as decoy agents to mitigate the uptake of the ENPs into macrophages differentiated from THP-1 monocytes. The decoy particles were intended to temporarily saturate the macrophages' uptake capacity [6,14].The LNCs were produced via phase inversion cycles [55]. Their hydrodynamic diameter was 41.65 ± 0.72 nm with a PDI of 0.036 ± 0.009 (mean ± SD from three independent batches). Their efficacy to modulate the ENP uptake into macrophages was assessed by flow cytometry experiments. Therefore, coadministration regimes (Fig. 2A, Fig. S2) of decoy LNCs and ENPs, aligned with previously published protocols in the literature [42], were tested on macrophages. The measured mean fluorescence intensity (APC-A geo. mean) served as an indicator for cell uptake of ENPs. LNC concentrations ranging from 3 nM to 0.3 nM were evaluated. The measurement of cell-associated fluorescence indicated that the uptake of ENPs into macrophages remained unchanged or increased following preincubation with LNCs compared to the control experiment using macrophages without preincubation (Fig. 2B, Fig. S2). Toxicity studies of LNCs were conducted on macrophages, revealing reduced cell

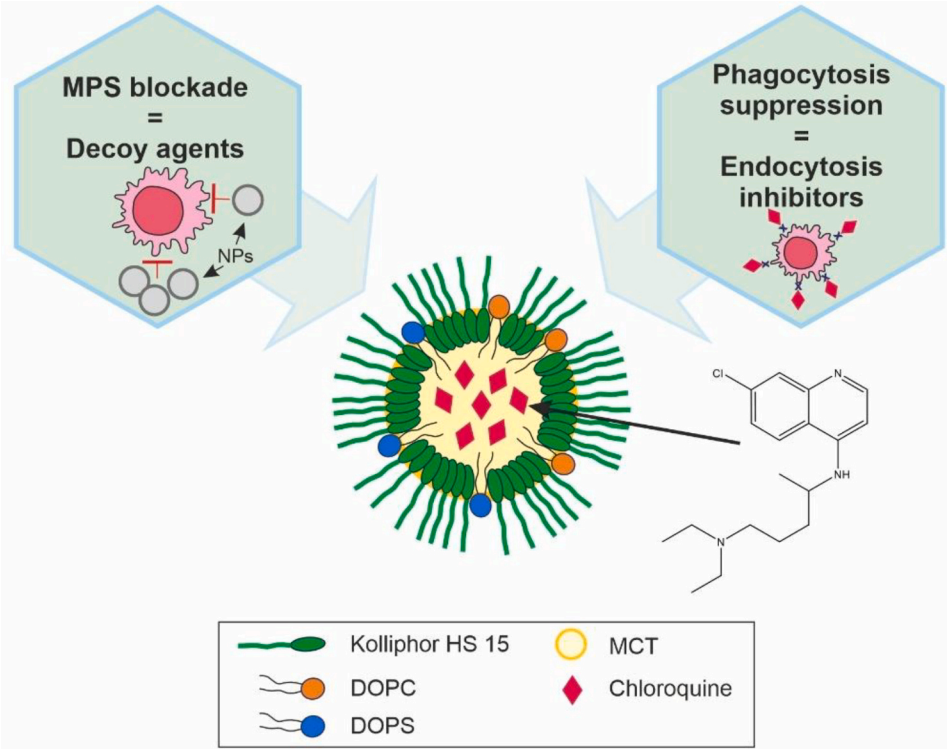

Fig. 1. Schematic depiction of the refined strategy to evade the clearance by the mononuclear phagocyte system (MPS) thereby enabling the implementation of subcutaneous administration regimes for ENPs. The previously described utilization of nanoparticulate decoy materials to block the MPS capacity by overload is shown as well as the application of endocytosis inhibitors to suppress the phagocytosis of ENPs. Both strategies result in a transient modulation of the immune system. In the present study, both approaches were combined to establish a refined strategy. Therefore, chloroquine was used as well-characterized endocytosis inhibitor and encapsulated into LNCs as decoy agents (100 % DOPC). Moreover, the effect of the incorporation of a targeting structure into the envelope of the LNCs (100 % DOPS) was evaluated for its efficiency to promote uptake inhibition of ENPs into macrophages.

viability following incubation with higher LNC concentrations for 24 h. The other tested LNC concentrations exhibited toxicity levels below the ISO cytotoxicity threshold (Fig. S3 A and B).

The effect of chloroquine diphosphate on the uptake of ENPs into macrophages was assessed in the same experimental setting. Its efficiency was analyzed within a concentration range (20–400 μM). This range was previously documented in the literature to be potent for nanoparticle uptake inhibition [33] across incubation intervals of 24 h to 1 h (Fig. S4A). The preincubation with chloroquine diphosphate resulted in a distinct inhibition of ENP uptake relative to the control, with increasing uptake inhibition at higher chloroquine diphosphate concentrations (200 μM, 400 μM) and extended preincubation durations (24 h). Lower chloroquine diphosphate concentrations showed uptake inhibition only after a preincubation period of 24 h as compared to the control. In subsequent experiments, it was assessed whether the uptake inhibition effect persisted even when the macrophages were incubated with ENPs for more than 0.5 h. It was demonstrated that chloroquine diphosphate reliably induced uptake inhibition for at least 2 h (Fig. S4B). The effect was thoroughly evaluated across a concentration range of ENPs from 1 nM to 1 pM by pretreating macrophages with chloroquine diphosphate at concentrations of 100 μM and 200 μM. Compared to the controls, the preincubated macrophages exhibited a significantly reduced uptake efficiency for ENPs across the entire concentration range over 4 h (Fig. 2C and D). Toxicity studies of the administration regime of chloroquine diphosphate and ENPs indicated toxicity levels below the ISO cytotoxicity threshold for chloroquine diphosphate at a concentration of 100 μM over 4 h, while a concentration of 200 μM resulted in decreased cell viability (Fig. S3C).

2.3. Chloroquine-loaded LNCs as refined decoy agents

To develop a refined strategy to mitigate ENP clearance by the MPS, chloroquine was encapsulated in LNCs, which have previously been validated as robust drug delivery systems [55,56]. Therefore, chloroquine diphosphate was converted into its free base via liquid–liquid extraction. The purity and identity of the chloroquine free base was verified against a commercially obtained reference using HPLC analysis (Fig. S5). Both, the extracted chloroquine free base and the reference showed a constant retention time of 2.9 min. To determine whether encapsulation of the endocytosis inhibitor in LNCs is feasible at therapeutically relevant concentrations, we calculated the dose required for immunomodulation in rats, a commonly used in vivo model. Compliance with standard administration volumes [57] and toxicity thresholds was ensured [5]. For an anticipated subcutaneous application volume of 250 μL, the concentration of encapsulated chloroquine had to be adjusted to 6 mg mL^{-1} per batch. *(The reader is referred to the supporting information)*. It was shown that chloroquine could be successfully encapsulated at concentrations exceeding therapeutically relevant levels. The encapsulation efficiency (*EE*) was determined to be 73.9 ± 7.5 % (mean ± SD; N = 2; n = 3) using HPLC analysis. The efficiency of chloroquine-loaded unmodified LNCs on the uptake inhibition of ENPs into macrophages was assessed in flow cytometry experiments. Therefore, the macrophages were preincubated with the LNCs according to the already established administration regime (Fig. 3A). The applied LNC concentrations were adjusted to obtain chloroquine concentrations of 100 μM, 200 μM and 300 μM. The corresponding LNC particle concentrations were ≤ 0.7 nM. The ENPs were applied at concentrations ranging from 0.1 nM to 0.01 nM and the mean fluorescence intensity (APC-A geo. mean) was assessed as an indicator for their uptake (Fig. 3B). The efficacy of chloroquine-loaded LNCs on the uptake

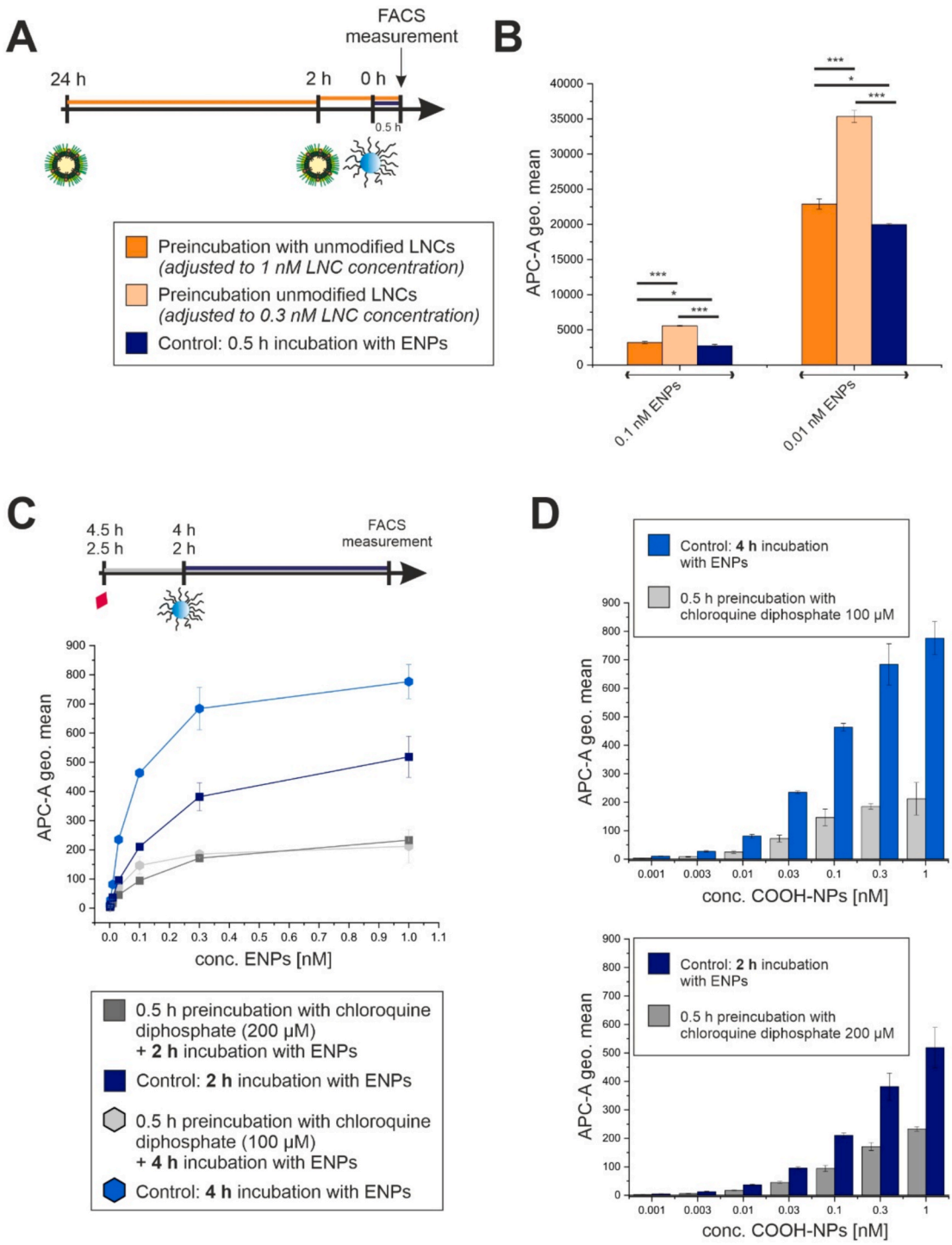

Fig. 2. Evaluation of unmodified LNCs as decoy agents and chloroquine diphosphate as endocytosis inhibitor. The mean fluorescence intensity (APC-A geo. mean) was assessed as an indicator for the uptake of CY-5-labeled ENPs into macrophages. Results represent mean ± SD (n = 3; n indicating replicates). Macrophages, which were treated exclusively with ENPs, without prior incubation with chloroquine diphosphate, served as control (indicated in blue). (A) Visualization of the administration regime: The macrophages were pretreated with either a dual application of unmodified LNCs for 24 h and 2 h or a single application for 2 h before the CY-5-labeled ENPs were added for further 0.5 h. (B) The mean fluorescence intensity (APC-A geo. mean) was quantified using flow cytometry analysis. Unmodified LNCs were applied at concentrations of 1 nM or 0.3 nM and the ENPs at concentrations of 0.1 nM and 0.01 nM. The statistical significance between means was evaluated with one-way ANOVA with subsequent Bonferroni corrected post hoc *t*-test, as the Levene test indicated variance homogeneity. Levels of statistical significance are indicated as n.s. – not significant, *$p \leq 0.05$, **$p \leq 0.01$, ***$p \leq 0.001$. (C) Visualization of the administration regime: Macrophages were preincubated with chloroquine diphosphate for 0.5 h before the ENPs were added for further 4 h or 2 h. Chloroquine diphosphate was applied at concentrations of 200 µM or 100 µM. The ENPs were applied in serial dilutions (1 nM to 1 pM). Controls are indicated in blue. (D) Evaluation of concentration-dependent effects on the uptake-inhibition of ENPs by chloroquine diphosphate. (For interpretation of the references to colour in this figure legend, the reader is referred to the web version of this article.)

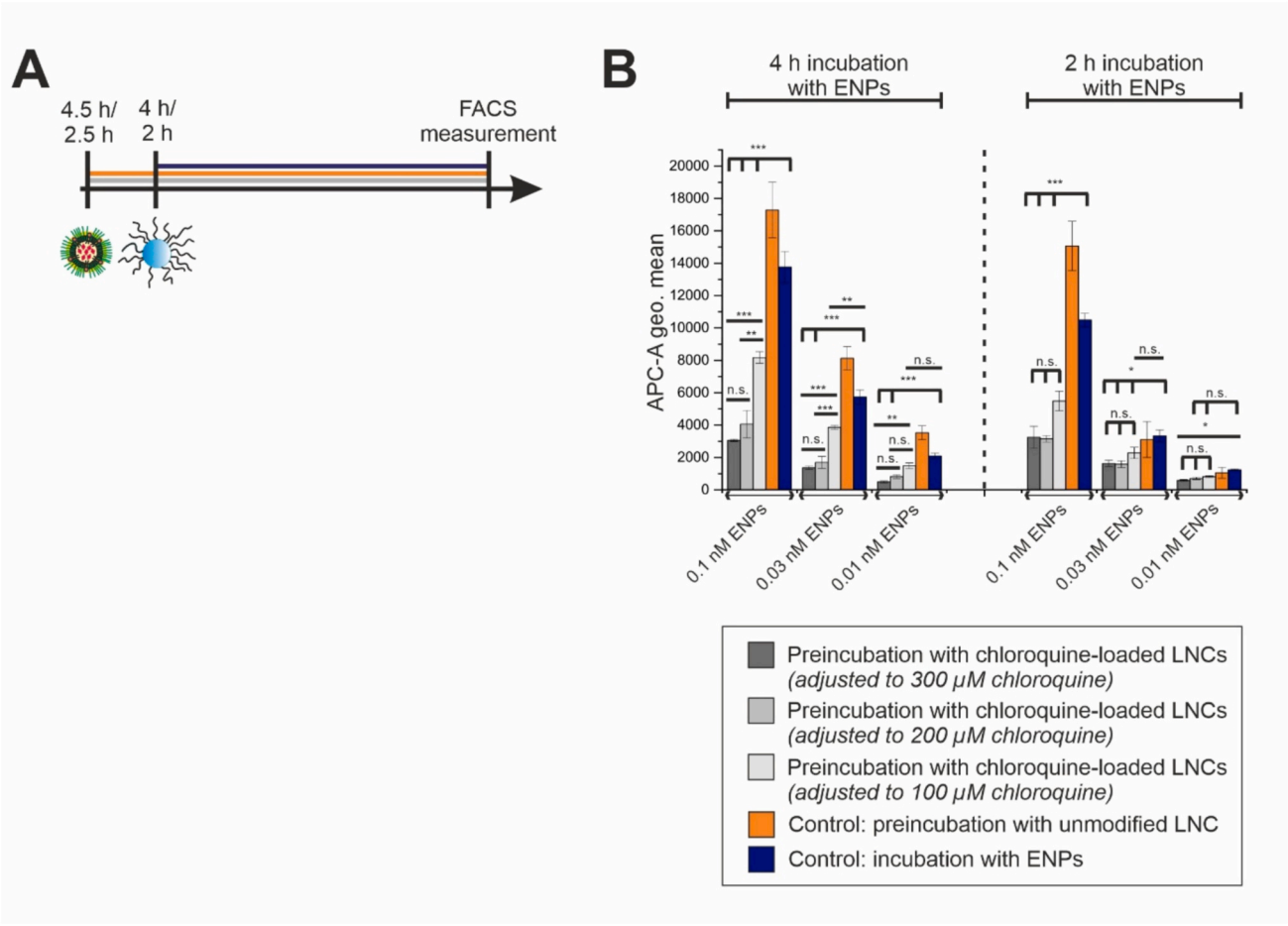

Fig. 3. Evaluation of chloroquine-loaded unmodified LNCs as decoy agents. (A) Visualization of the administration regime: The macrophages were pre-incubated with chloroquine-loaded unmodified LNCs for 0.5 h before subsequent incubation with CY-5-labeled ENPs for 4 h or 2 h. (B) The mean fluorescence intensity (APC-A geo. mean) was assessed as an indicator for the uptake of ENPs into macrophages. Results represent mean ± SD (n = 3; n indicating replicates). Macrophages, which were treated exclusively with ENPs, without prior incubation with chloroquine-loaded LNCs, and macrophages, which were pretreated with unloaded LNCs before incubation with ENPs served as control. The statistical significance between means was evaluated with one-way ANOVA with subsequent Bonferroni corrected post hoc *t*-test, as the Levene test indicated variance homogeneity. Levels of statistical significance are indicated as n.s. – not significant, *p ≤ 0.05, **p ≤ 0.01, ***p ≤ 0.001.

inhibition was examined with one-way ANOVA with subsequent Bonferroni corrected post hoc *t*-test, as the Levene test indicated variance homogeneity. Preincubation with chloroquine-loaded unmodified LNCs resulted in a statistically significant reduction ENP uptake over 4 h compared to macrophages that were not preincubated. As an additional control experiment, macrophages were preincubated with unloaded LNCs, which resulted in either unchanged or increased uptake of ENPs compared to the control.

2.4. The effect of engineered LNCs

1,2-Dioleoyl-*sn*-glycero-3-phosphoserine (DOPS) was incorporated as a targeting structure into the decoy LNCs (= engineered LNCs) to provide an additional uptake stimulus for macrophages [48]. Therefore, 1,2-dioleoyl-*sn*-glycero-3-phophocholine (DOPC) was partially replaces by DOPS during the production of LNCs (Fig. 4A). The engineered LNCs, with DOPS contents ranging from 25 % to 100 % (m/m), exhibited hydrodynamic diameters between 40.08 ± 0.01 nm and 42.94 ± 0.45 nm along with PDIs ranging from 0.03 ± 0.01 to 0.07 ± 0.02 (mean ± SD from three independent batches) (Fig. 4B). To assess the uptake-enhancing effect of DOPS, the LNCs were stained with DiO and added to macrophages for 0.5 h and 1 h. Unmodified LNCs (0 % DOPS) served as control. The mean fluorescence intensity (APC-A geo. mean) was measured via flow cytometry experiments and assessed as an indicator for the uptake of engineered LNCs into macrophages (Fig. 4C). In both experimental settings, a statistically significant difference in the uptake of LNCs into macrophages was only observed for DOPS contents of at least 75 %. Subsequently, further investigations were conducted using LNCs, in which the DOPC was substituted quantitatively with DOPS (100 %-DOPS-LNCs).

Chloroquine free base was encapsulated into 100 %-DOPS-LNCs. Using HPLC analysis, the *EE* was determined to be 88.0 ± 27.0 % (mean ± SD; N = 2; n = 3; N indicating samples, n indicating replicates). The chloroquine-loaded 100 %-DOPS-LNCs differed statistically significantly in their size from unmodified chloroquine-loaded LNCs (two sample *t*-test: p-value = 6.424×10^{-7}) (Fig. 5A). To compare their effect on the uptake inhibition of ENPs, the previously described experimental settings and administration regimes for flow cytometry experiments were employed (Fig. 5B). The applied concentrations of both LNC types were adjusted to chloroquine concentrations of 200 µM. The corresponding LNC particle concentrations were ≤ 0.7 nM. Macrophages, which were preincubated with 200 µM chloroquine diphosphate were set as an additional control. Preincubation with chloroquine-loaded 100 %-DOPS-LNCs and chloroquine-loaded unmodified LNCs resulted in a statistically significant reduction of ENP uptake over 4 h compared to macrophages that were not preincubated with chloroquine-loaded LNCs (Fig. 5C). Compared to macrophages that were preincubated with chloroquine diphosphate, the difference in ENP uptake over 4 h was

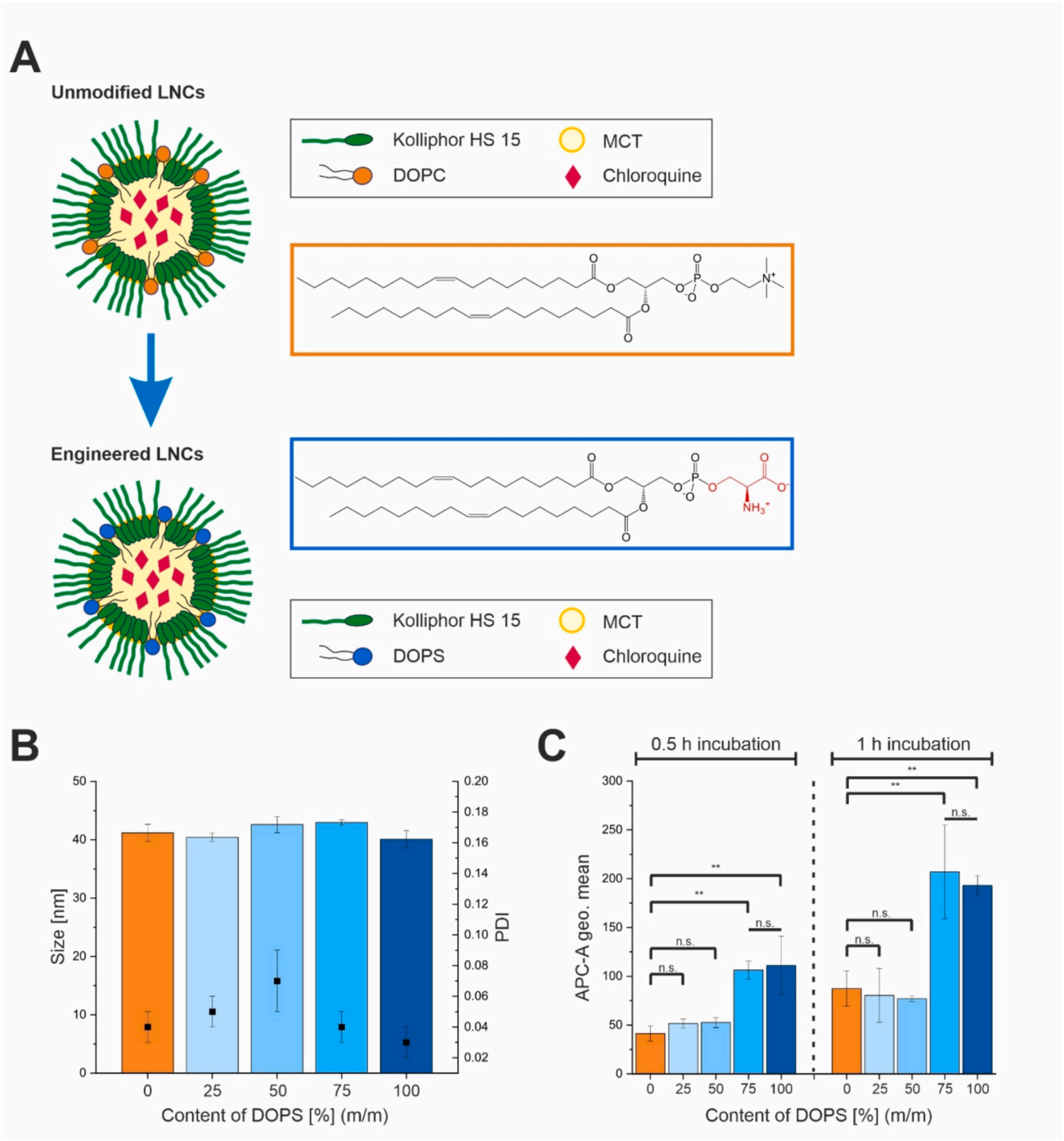

Fig. 4. Engineering LNCs with DOPS as "eat-me" signal to trigger their phagocytosis. (A) Schematic illustration of the chemical composition of unmodified and engineered LNCs and the chemical structures of DOPC and DOPS. (B) Size [nm] and PDI of LNCs with varying contents of DOPS [%] (m/m). DLS data represent mean ± SD (N = 3; n = 3; N indicating samples, n indicating replicates). (C) Investigation of the LNC uptake into macrophages as a function of their DOPS content [%] (m/m). Results represent mean ± SD (n = 3; n indicating replicates). The statistical significance between means was evaluated with one-way ANOVA with subsequent Bonferroni corrected post hoc *t*-test, as the Levene test indicated variance homogeneity. Levels of statistical significance are indicated as n.s. – not significant, *p ≤ 0.05, **p ≤ 0.01, ***p ≤ 0.001.

statistically weakly significant or not significant. Furthermore, the analysis of the flow cytometry experiments revealed that preincubation with unloaded, drug-free 100 %-DOPS-LNCs compared to unloaded unmodified LNCs, did not reduce the uptake of ENPs into macrophages but instead significantly increased it.

3. Discussion and conclusion

In the present study, we developed a synergistic co-administration strategy with chloroquine-loaded LNCs to reduce ENP clearance by immune cells. Following an engineering-driven approach, the ENPs were protected against excessive opsonization by PEGylation of their surface [19,50,58]. The coadministration regime with endocytosis inhibitor-loaded LNCs was aimed to further reduce the clearance of the

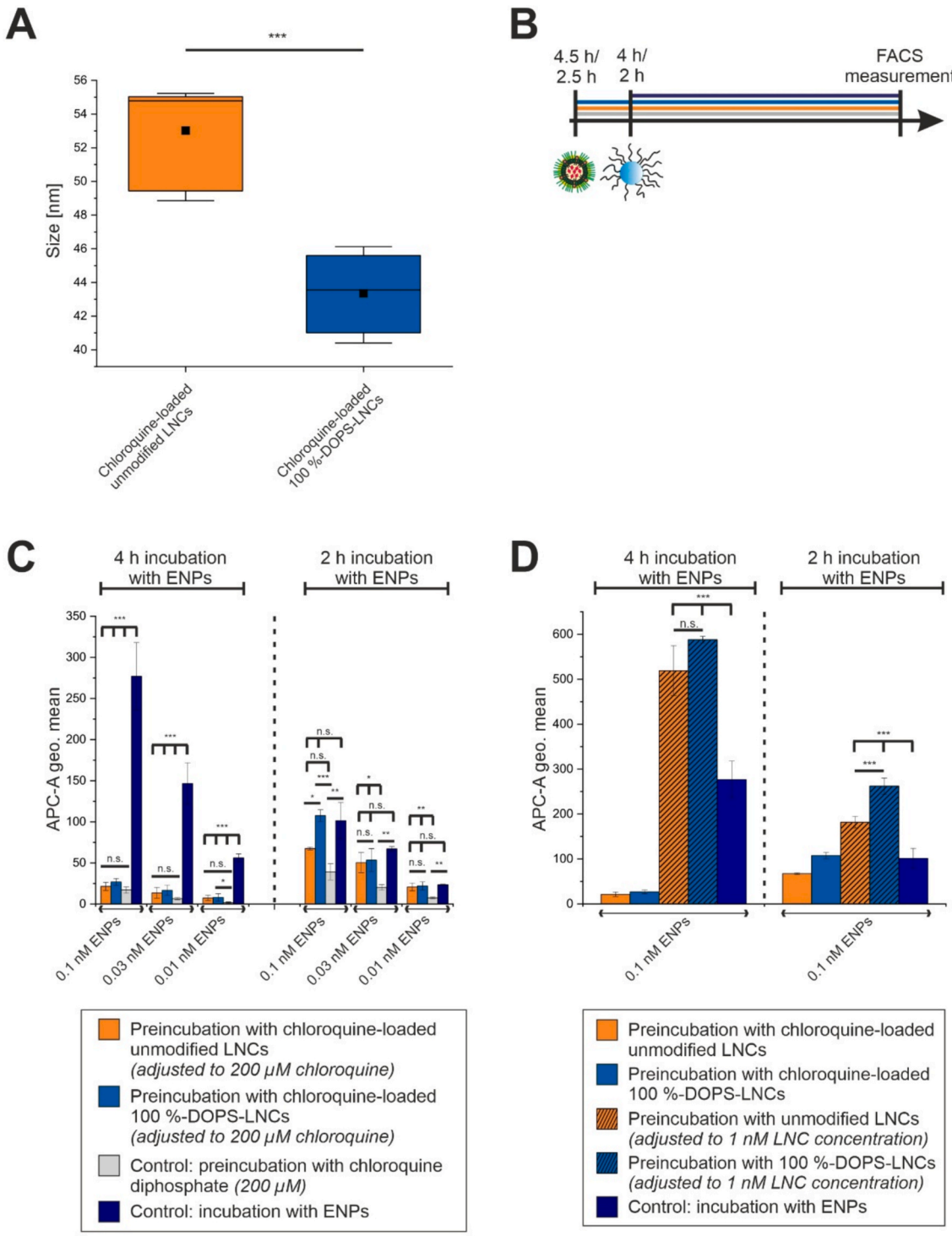

Fig. 5. Evaluation of engineered chloroquine-loaded LNCs as decoy agents. (A) Size [nm] of chloroquine-loaded unmodified LNCs and chloroquine-loaded 100 %-DOPS-LNCs. DLS data represent mean ± SD (from three independent batches). Derived means were compared via two sample *t*-test (p-value = 6.424×10^{-7}). Levels of statistical significance are indicated as n.s. – not significant, *p ≤ 0.05, **p ≤ 0.01, ***p ≤ 0.001. (B) Visualization of the administration regime: The macrophages were pre-incubated with chloroquine-loaded unmodified LNCs and chloroquine-loaded 100 %-DOPS-LNCs for 0.5 h before subsequent incubation with ENPs for 4 h or 2 h. (C) The mean fluorescence intensity (APC-A geo. mean) was assessed as an indicator for the ENPs into macrophages. Macrophages, which were treated exclusively with ENPs, without prior incubation with decoy agents, served as control. Results represent mean ± SD (n = 3; n indicating replicates). The statistical significance between means was evaluated with one-way ANOVA with subsequent Bonferroni corrected post hoc *t*-test, as the Levene test indicated variance homogeneity. Levels of statistical significance are indicated as n.s. – not significant, *p ≤ 0.05, **p ≤ 0.01, ***p ≤ 0.001. (D) Comparison of the uptake of ENPs after preincubation with chloroquine-loaded unmodified LNCs, chloroquine-loaded 100 %-DOPS-LNCs, unmodified LNCs and 100 %-DOPS-LNCs. Results represent mean ± SD (n = 3; n indicating replicates). The statistical significance between means was evaluated with one-way ANOVA with subsequent Bonferroni corrected post hoc *t*-test, as the Levene test indicated variance homogeneity. Levels of statistical significance are indicated as n.s. – not significant, *p ≤ 0.05, **p ≤ 0.01, ***p ≤ 0.001.

ENPs by transiently suppressing immune cells's phagocytic activity. Chloroquine, as FDA-approved drug, was chosen as endocytosis inhibitor for this approach. The drug interferes with the clathrin-mediated endocytosis of nanoparticles, which, in addition to phagocytosis, represents an important uptake mechanism for nanoparticles into macrophages [33]. In a previous study, we were able to demonstrate that clathrin coated pits, and consequently clathrin mediated endocytosis, play a pivotal role in the interaction of polymer nanoparticles and cell surfaces [59]. LNCs were selected as carrier system to promote the chloroquine uptake via the lymph, as they showed excellent encapsulation efficiency for lipophilic drugs [55,56]. Their small size and narrow size distribution confer accelerated uptake from the subcutaneous tissue relative to the larger ENPs [60] resulting in an expected temporally advanced immunomodulation. Moreover, as particulate systems, they exhibit a high potential for interaction with MPS cells [6,14]. Several studies have already demonstrated that the administration of high doses of non-toxic, unloaded (drug-free) nanoparticles as decoy agents leads to saturation of the uptake capacity of MPS cells, which results in a reduced uptake of subsequently administered ENPs [6,14]. However, saturation effects could not be proven after preincubation with the decoy particles in the present study. This could be attributed to the utilized decoy nanoparticle concentrations. Ouyang et al. [61] demonstrated that the threshold for the uptake capacity of Kupffer cells, which are liver specific macrophages, in mice was reached at 1 trillion (gold) nanoparticles. Once this threshold was exceeded, the clearance of systemically administered nanoparticles significantly decreased. However, this threshold did not represent the total capacity of the cells but a kinetic limit. In vitro, the uptake leveled off at 100,000 phagocytosed nanoparticles per cell over 24 h (applied nanoparticle concentration: approximately 1.0×10^{12} particles mL^{-1}). In the present study, the administered decoy nanoparticle concentrations were lower by at least a factor of 1000 due to toxicity considerations. The toxicity of high doses of unloaded decoy particles has already been critically evaluated as a health risk in the literature [62,63]. The encapsulation of chloroquine made the decoy LNCs effective even at moderate, in vitro non-toxic concentrations. Chloroquine possesses an acceptable toxicity profile and has already been utilized as an adjuvant therapy in combination with chemotherapy for extended treatment durations [33,64]. The endocytosis-inhibitory effect on cells is transient. The cells can fully regenerate after the removal of chloroquine. This is highly relevant for the prospective administration in vivo, as a persistent impairment of the immune system would pose significant health risks [65].

To gain deeper insights into the translational potential of this refined synergistic approach, we investigated the incorporation of a macrophage-specific targeting signal for its effectiveness. This did not require any modification of the ENP structure, as the targeting signal was integrated into the envelope of the decoy LNCs. Previously, Tang and coworkers published an approach [66], in which a CD47-derived peptide ligand was integrated into the decoy particle structure to block the surface of macrophages by specific ligand-receptor interactions. Consequently, their system was not based on the intracellular release of a MPS modulator from the decoy particles. In contrast, we investigated the incorporation of DOPS as a targeting signal which was intended to promote the specific uptake of the decoy LNCs into macrophage for a subsequent increased intracellular chloroquine-release. DOPS is an "eat-me" signal presented by apoptotic cells [46] and is utilized by certain viruses for cell targeting [47,67]. It has already been successfully employed as a ligand-like structure in particulate systems to target macrophages [48]. However, the results obtained in this study indicate that its incorporation in the decoy LNCs did not enhance their efficacy of uptake-inhibition for ENPs in vitro. In vivo, however, it may exert advantageous effects, as phosphatidylserine not only promotes uptake by phagocytic cells but also induces anti-inflammatory responses [68]. Therefore, it can be considered advantageous that the use of decoy nanomaterials in synergistic approaches allows for the ENP-independent incorporation of targeting ligands. However, further development is still required at this stage. Another advantage of endocytosis inhibitor-loaded decoy-LNCs in co-administration is that it enables subcutaneous administration of ENPs. This, however, requires effective inhibition of phagocytic immune cells in the lymph nodes. Due to its molecular weight (< 1 kD), unencapsulated chloroquine would not be quantitatively absorbed via the lymph vessels after subcutaneous administration. Instead, it would enter the systemic circulation through small blood capillaries [69]. Accordingly, its encapsulation in decoy particles at therapeutically relevant concentrations is essential for targeted release into lymph macrophages and subsequent inhibition of their phagocytic activity.

So far, various synergistic coadministration regimes with endocytosis inhibitors or decoy nanomaterials have been published. However, these approaches have quantitatively been developed for systemic (intravenous) administration regimes to modulate the target/off-target distribution of ENPs [62,70,71]. To the best of our knowledge there is only one study in which a coadministration regime with endocytosis inhibitor-loaded decoy particles was utilized to render ENPs systemically available after subcutaneous administration [42]. Stack et al. [42] successfully employed lantrunculin A-loaded micelles as decoy particles for subsequent subcutaneous ENP administration. For their system, they demonstrated reversible, non-toxic MPS inhibition, achieving serum ENP levels after subcutaneous coadministration comparable to those following intravenous administration. Lantrunculin A, a micropinocytosis inhibitor, has so far only been utilized in research and has not been approved as a drug substance. Both, the employed decoy particles and the ENPs were composed of the same polymer, poly(ethylene glycol)-*block*-poly(propylene sulfide) (PEG-b-PPS). In present study, we differentiate our approach by utilizing nanoparticles, which differ from micelles by higher stability and, consequently, enhanced suitability as carrier systems [72]. Moreover, we employed two distinct particle types, lipid-based decoy particles and polymeric ENPs. With this, our study provides an initial indication of the general transferability of this concept between different nanoparticle types. It is therefore conceivable that an established decoy nanoparticle system could be combinable with various ENPs, which are optimized for their targets.

Furthermore, nanoparticles have so far only been administered subcutaneously as depots for the sustained release of their cargo [69,73–75]. For this purpose, the sizes of the nanoparticles (> 100 nm) were chosen to prevent their entry into the lymphatic system, ensuring the release of the loaded drugs into the subcutaneous tissue [69]. Following subcutaneous administration, drug substances first pass the interstitium to reach the lymphatic vessels and blood capillaries [69]. Their encapsulation within nanoparticles further amplifies this naturally occurring retardation effect by the influence of the release kinetics from the nanoparticle depot. However, if the entire nanoparticle successfully reaches the systemic circulation after subcutaneous administration, a retardation effect could be expected compared to its intravenous administration. This may prove advantageous for the targeting efficiency of the nanoparticles as drug delivery systems [76]. Furthermore, it improves their toxicity profiles as it prevents an overload of the liver, which typically occurs after systemic administration [63]. Hence, refined coadministration regimes with encapsulated endocytosis inhibitors in decoy particles may provide the foundation for establishing a novel application route for nanoparticles, enabling their sustained release into systemic circulation. The subcutaneous application of nanoparticles would therefore no longer be limited to its use as drug-releasing depots. Since the coadministration regime incorporates the application of an endocytosis-inhibitor loaded decoy nanoparticle alongside the PEGylation of the ENPs, this approach can be furthermore applied to various ENPs.

4. Material and methods

4.1. Materials

All materials and reagents were purchased from Sigma Aldrich (Taufkirchen, Germany or St. Louis, USA) unless otherwise stated. Dulbecco's phosphate-buffered saline (DPBS) was acquired from Gibco™ (Life Technologies, Paisly, UK). The ultrapure water used for the experiments was produced with a Milli-Q EQ 7000 system (Merck, Darmstadt, Germany) equipped with Milli-Q Biopak filter (Merck, Darmstadt, Germany) and freshly taken every day. It is referred to as Milli-Q water in the following.

4.2. Cell culture

Human acute monocytic leukemia cells (THP-1 monocytes) were cultured in RPMI 1640 cell culture medium (gibco, RPMI Medium 1640 (1X), [-]-L-Glutamine, Thermofisher, Paisley, UK) containing 10 % fetal bovine serum (FBS) (South America Origin, Pan-Biotech, Aidenbach, Germany, Lot-No.: P201004) and supplemented with MEM non-essential amino acids, MEM vitamins, sodium pyruvate and glutamine (gibco, Life Technologies Corporation, Grand Island, USA). For the differentiation into macrophages, 100 nM phorbol-12-myristate-13-acetate (PMA) (ThermoScientific Fisher, Schwerte, Germany) was added to the cell culture medium 48 h before the experiment. The cells were cultured in a water saturated, carbon dioxide enriched (5 % CO_2) atmosphere at 37 °C.

4.3. Nanoparticle Preparation

Core-shell nanoparticles were obtained by nanoprecipitation as previously described [43,77]. For this purpose, the synthesized PLA_{10K}-PEG_{5K}-COOH block-copolymer was dissolved together with CY-5 labeled PLGA (CY-5-PLGA) in acetonitrile (ACN) to a concentration of 10 mg mL^{-1}. The ratio of the CY-5-PLGA core to block-copolymer shell was 3:7 (m/m). The organic phase was added dropwise into the 10-fold excess of stirring (930 rpm) aqueous phase (10 % DPBS (v/v) in Milli-Q water) and stirred for 3 h to remove the ACN. Subsequently, the volume was concentrated by centrifugation at 3000 g for 15 min using Microseps Advance 30 K centrifugal filters (molecular weight cut-off 30 kDa, Pall Corporation, New York, USA).

4.4. Lipid nanocapsules (LNC) preparation

LNCs were manufactured as previously published [78]. For unmodified LNCs, 295.8 mg Kolliphor® HS15 solution 40 % (m/m) in Milli-Q water, 18.3 mg (13.3–23.3 mg) 1,2-dioleoyl-*sn*-glycero-3-phosphocholine (DOPC, LIPOID PC 18:1/18:1, kindly provided by LIPOID GmbH, Ludwigshafen, Germany), 138.3 mg Miglyol® (Miglyol® 812, Ph.Eur.8.0, Caesar & Loretz GmbH, Hilden, Germany) and 222.6 mg aqueous NaCl solution (50 mg mL^{-1}) were mixed and subjected to three heating (to 90 °C)-cooling (to 60 °C) cycles. In the last cooling cycle 850 µL aqueous NaCl solution were added at the phase inversion temperature (approx. 76 °C) to form stable LNCs. The LNC emulsion was stirred for further 5 min and then sterile filtered through a RC-filter (0.22 µm) to remove excess lipid. The LNC emulsion was stored at 2–8 °C protected from light. For engineered LNCs, DOPC was replaced proportionately by 1,2-dioleoyl-*sn*-glycero-3-phosphoserine, sodium salt (DOPS-Na, LIPOID PS 18:1/18:1, kindly provided by LIPOID GmbH, Ludwigshafen, Germany) and the manufacturing process was completed as described above. For selected flow cytometry experiments, the LNCs were labeled with DiO (DiOC18(3), Invitrogen, Thermo Fisher Scientific, OR, USA). In this case, 0.5 mg DiO were added to the mixture before it underwent the heating–cooling cycles.

	Amount of **DOPC [%]**	Amount of **DOPS [%]**
Unmodified LNCs	100	0
Engineered LNCs	75	25
	50	50
	25	75
	0	100

4.5. Nanoparticle and LNC characterization

4.5.1. Nanoparticle characterization

Dynamic light scattering (DLS)-based measurements (particle size distribution, polydispersity index) were carried out with a Malvern Zetasizer Nano ZS (Malvern Instruments, Herrenberg, Germany) equipped with a λ 633 nm He-Ne laser operating at an angle of 173° [43,77]. The software used for data collecting and processing was Zetasizer software version 7.12 (Malvern Instruments, UK). To determine the size distribution, the concentrated samples were diluted 1:20 with 10 % DPBS in Milli-Q water (10 % DPBS (v/v)). 90 µL sample volume were measured in micro-UV-cuvettes (Carl Roth, Karlsruhe, Germany) at a controlled temperature of 25 °C (120 sec equilibration time). Three repetitions with 11 runs of 10 sec duration were performed for each sample. The data was analyzed with the software-integrated analysis model for "general purposes (normal resolution)".

Furthermore, average size (hydrodynamic diameter) and concentration [particles mL^{-1}] of the nanoparticles were determined using nanoparticle tracking analysis (NanoSight NS300, Malvern, Worcestershire, UK). The device was equipped with an O-Ring top-plate and the data was analyzed with NanoSight NTA 3.4 software (NTA Malvern Panalytical software). Before measurement, all samples were diluted with Milli-Q water to achieve a good particle per frame value (20–100 particles/frame). The samples were applied by manual injection with sterile syringes. Each sample was measured in three cycles of 60 sec duration (screen gain: 1.0; camera level: 16) at RT. The detection threshold was set at 3.

4.5.2. LNC characterization

Particle size distribution and polydispersity index measurements were carried out with a Malvern Zetasizer Nano ZS as for the polymeric nanoparticles. Therefore, the LNC samples were diluted 1:20 with 10 % DPBS in Milli-Q water. 90 µL sample volume were measured in micro-UV-cuvettes (Carl Roth, Karlsruhe, Germany) at a controlled temperature of 25 °C (120 sec equilibration time). Three repetitions with 11 runs of 10 sec duration were performed for each sample. The data was analyzed with the software-integrated analysis model for "general purposes (normal resolution)". Furthermore, average size (hydrodynamic diameter) and concentration [particles mL^{-1}] were determined using nanoparticle tracking analysis as described above. Before measurement, the samples were diluted with Milli-Q water. The samples were applied by manual injection with sterile syringes. Each sample was measured in three cycles of 60 sec duration (screen gain: 1.0; camera level: 16) at RT. The detection threshold was set at 2.

4.6. Chloroquine free base synthesis and characterization

About 1 g of the chloroquine diphosphate salt was placed in the separating funnel, and the free base of the drug was extracted by liquid–liquid extraction with ethyl acetate (50 mL) and sodium hydroxide solution (2 M, 75 mL). The organic layer was separated and shaken again against sodium hydroxide solution (1 M, 75 mL). The solvent was then removed under vacuum for 12 h. Identity and purity of the chloroquine free base were verified by high performance liquid chromatography (HPLC) analysis. HPLC analyses were performed on an Agilent Technologies 1260 Infinity ll (Santa Clara, USA). For this, a C18 column

(CORTEX T3 2.7 μm, 3 x 100 mm column) was used, that was heated to 40 °C. Acetonitrile (HPLC grade) [A] and 0.1 % triethylamine in Milli-Q water (pH 3.0 adjusted with phosphoric acid) [B] were employed as the mobile phases for the gradient elution at a flow rate of 1.0 mL min^{-1} as previously published by Miranda et al. [79]. The following gradient was applied: [A] at 5 % – 0–2 min/ [A] 5 to 40 % – 2–4 min/ [A] at 40 % – 4–5.3 min/ [A] 40 to 5 % – 5.3–7 min/ [A] at 5 % – 7–9 min. Fluorescence detection was performed at excitation λ 325 nm and emission λ 375 nm. Emission spectra were recorded in the peaks (scan range: λ 335 nm to 400 nm, step: 10 nm). 2 μL sample volume (dissolved in methanol and aqueous phase [B], ratio 1:1) were applied in each run. The extracted chloroquine free base showed a constant retention time of 2.9 min and was compared to chloroquine free base (reference) purchased from MedChemExpress (Hölzel Diagnostika Handels GmbH, Köln, Germany).

4.7. Chloroquine encapsulation and quantification via HPLC analysis

To prepare chloroquine-loaded LNCs, 24 mg chloroquine were dissolved in dichloromethane and added to the mixture of Kolliphor® HS15, Miglyol® and DOPC/DOPS. The dichloromethane was evaporated at 75 °C for 30 min. The aqueous NaCl solution was then added, and the heating–cooling-cycles were initiated as described above. Free non-encapsulated chloroquine was separated by centrifuging the LNC batches twice (*2x* addition of 1.0 ml Milli-Q water for washing, centrifugation at 4500 g for 30 min) using Microseps Advance 30 K centrifugal filters (molecular weight cut-off 30 KDa, Pall Corporation, New York, USA). The resulting filtrate was adjusted to a final volume of 2.0 mL with Milli-Q water. 200 μL of the LNC emulsion were diluted 10-fold with methanol and ultrasonicated for 30 min to disrupt the LNC structure and to release the drug, which was quantified by HPLC analysis. Therefore, 100 μL of the sample were diluted with 100 μL mobile phase [B] (0.1 % triethylamine in Milli-Q water (pH 3.0 adjusted with phosphoric acid)). The HPLC analysis was performed as described above for the free chloroquine base. However, the gradient was extended to reliably elute the lipids from the HPLC column, which had no effect on the retention time of the chloroquine base. The following gradient was applied: [A] at 5 % – 0–2 min/ [A] 5 to 40 % – 2–4 min/ [A] at 40 % – 4–5.3 min/ [A] 40 to 90 % – 5.3–9 min/ [A] 90 to 5 % – 9–10 min/ [A] at 5 % – 10–15 min. The samples were analyzed in triplicate and the mean drug content [mg mL^{-1}] (mean ± SD; n = 3) was calculated using a previously recorded calibration curve (chloroquine conc.: 0.1 – 0.8 mg mL^{-1}) with the regression coefficient of $R^2 = 0.9989$. The encapsulation efficiency (*EE*) was calculated as depicted in Eq. (1), with m_e referring to the mass of encapsulated drug and m_a referring to the mass of initially added drug:

$$EE[\%] = \frac{m_e}{m_a} \bullet 100 \quad (1)$$

4.8. Flow cytometry

THP-1 monocytes were seeded into 48-well plates at a density of 120,000 cells/well. The monocytes were differentiated into macrophages by addition of 100 nM PMA to the cell culture medium and incubated for 48 to 72 h (37 °C, 5 % CO_2) before proceeding the flow cytometry experiment. At the day of the experiment, the cells were washed with pre-warmed DPBS before preincubation with the decoy agents (unmodified and unstained LNCs, conc.: 3 nM, 1 nM, 0.3 nM/ engineered LNCs, conc.: 1 nM) or the endocytosis inhibitor (aqueous chloroquine dilution (chloroquine diphosphate) conc.: 20 μM, 100 μM, 200 μM, 400 μM) [33] or the endocytosis inhibitor containing *LNCs* (chloroquine containing unmodified or engineered LNCs, adjusted to chloroquine conc. of 100 μM, 200 μM, 300 μM chloroquine) under moderate shaking (50 rpm) at 37 °C for 0.5–24 h. After pre-incubation, CY-5-labeled ENPs were added to the wells without discarding the previously applied material and incubated under moderate shaking (50 rpm) at 37 °C for 0.5–4 h. To determine concentration-dependent effects, serial dilutions (1 nM to 1 pM, final nanoparticle concentration in the cell culture well) of ENPs were prepared in RPMI 1640 medium containing FBS. For the remaining experiments, the ENP concentrations were adjusted to 0.1 nM, 0.03 nM and 0.01 nM (final nanoparticle concentration in the cell culture well). To determine the effect of LNC engineering with different amounts of DOPS, the cells were incubated with the DiO-stained LNCs for 30 min or 1 h. Owing to the uniformity of the manufacturing process, the concentrations of all batches were considered equivalent. The LNC batches were diluted in the same ratio (1:66.7) with RPMI 1640 medium containing FBS.

After the incubation period, the medium was discarded, and for harvesting, 300 μL of trypsin (0.25 %) (PAN-Biotech, Aidenbach, Germany) were added and the cells were incubated for 2 min (37 °C, 5 % CO_2). After cell detachment, 500 μL of ice-cold RPMI 1640 were added to quench trypsinization. The samples were transferred to 2.0 ml Eppendorf-Tubes and centrifuged (0.3 g, 7 min, 4 °C). The supernatant was discarded, and the cells were washed twice with ice-cold DPBS under centrifugation. The cell pellets obtained after the last washing step were resuspended in 200 μL ice-cold DPBs and kept on ice until measurement. Flow cytometry analyses were performed on a FACS Canto ll (Becton Dickinson, Franklin Lakes, USA). The fluorescence of the CY5-labelled NPs was excited at λ 633 nm and the emission was recorded using a λ 661/16 nm bandpass filter. The fluorescence of the DiO-stained LNCs was excited at λ 488 nm and the emission was recorded using a λ 530/30 nm bandpass filter. The data was analyzed and plotted using Flowing software (v2.5.1, Cell Imaging and Cytometry Core, Turku Bioscience Centre, Turku, Finland, with the support of Biocenter Finland). Further evaluations were carried out based on the determined geometric mean of the fluorescence intensity.

4.9. Statistics

The statistical significance between means was evaluated with two sample *t*-test or one-way ANOVA with subsequent Bonferroni corrected post hoc *t*-test using R software. The data was tested for variance homogeneity using Levene test, before.

4.10. Software

The software used for the different experiments is listed below.

TopSpin 4.1.4 software (Bruker Corporation/Billercia/MA/USA, URL: https://www.bruker.com/en/products-and-solutions/mr/nmr-software/topspin.html) was used for NMR processing and analysis.

Origin 2022b software (OriginLab Corporation/Northampton/Ma/USA. URL: https://www.originlab.com/2022b) was used for data plotting and analyzing.

Flowing software (v2.5.1, Cell Imaging and Cytometry Core, Turku Bioscience Centre, Turku, Finland, with the support of Biocenter Finland. URL https://flowingsoftware.com/download/) was used for FACS data analyses and plotting.

R software (R Core Team (2022). R: A language and environment for statistical computing. R Foundation for Statistical Computing, Vienna, Austria. URL https://www.R-project.org/) was used for data plotting and statistical analysis.

CRediT authorship contribution statement

Kathrin Schorr: Writing – review & editing, Writing – original draft, Visualization, Project administration, Methodology, Investigation, Formal analysis, Data curation, Conceptualization. **Johannes Konrad:** Methodology. **Jan Birringer:** Methodology. **Carsten Damm:** Methodology. **Miriam Breunig:** Writing – review & editing, Visualization. **Achim Goepferich:** Writing – review & editing, Writing – original draft, Supervision, Validation, Project administration, Funding acquisition,

Conceptualization.

Declaration of competing interest

The authors declare the following financial interests/personal relationships which may be considered as potential competing interests: Given her role as Editor-in-Chief, Miriam Breunig had no involvement in the peer review of this article and had no access to information regarding its peer review. Full responsibility for the editorial process for this article was delegated to another journal editor. If there are other authors, they declare that they have no known competing financial interests or personal relationships that could have appeared to influence the work reported in this paper.

Acknowledgements

The authors like to kindly thank the German Research Foundation (DFG) for financial support, grant GO 565/22-1.

Appendix A. Supplementary data

Supplementary data to this article can be found online at https://doi.org/10.1016/j.ejpb.2026.114989.

Data availability

Data will be made available on request.

References

[1] M.J. Mitchell, M.M. Billingsley, R.M. Haley, M.E. Wechsler, N.A. Peppas, R. Langer, Engineering precision nanoparticles for drug delivery, Nat. Rev. Drug Discov. 20 (2021) 101–124, https://doi.org/10.1038/s41573-020-0090-8.
[2] D. Mishra, J.R. Hubenak, A.B. Mathur, Nanoparticle systems as tools to improve drug delivery and therapeutic efficacy, J. Biomed. Mater. Res. A 101 (2013) 3646–3660, https://doi.org/10.1002/jbm.a.34642.
[3] Role of nanoparticles in drug delivery system: a comprehensive review, 2017.
[4] S. Wilhelm, A.J. Tavares, Q. Dai, S. Ohta, J. Audet, H.F. Dvorak, W.C.W. Chan, Analysis of nanoparticle delivery to tumours, Nat. Rev. Mater. 1 (2016), https://doi.org/10.1038/natrevmats.2016.14.
[5] J.A. Mills, J. Humphries, J.D. Simpson, S.E. Sonderegger, K.J. Thurecht, N. L. Fletcher, Modulating macrophage clearance of nanoparticles: comparison of small-molecule and biologic drugs as pharmacokinetic modifiers of soft nanomaterials, Mol. Pharm. 19 (2022) 4080–4097, https://doi.org/10.1021/acs.molpharmaceut.2c00528.
[6] J.A. Mills, F. Liu, T.R. Jarrett, N.L. Fletcher, K.J. Thurecht, Nanoparticle based medicines: approaches for evading and manipulating the mononuclear phagocyte system and potential for clinical translation, Biomater. Sci. 10 (2022) 3029–3053, https://doi.org/10.1039/d2bm00181k.
[7] E. Samuelsson, H. Shen, E. Blanco, M. Ferrari, J. Wolfram, Contribution of Kupffer cells to liposome accumulation in the liver, Colloids Surf. B Biointerfaces 158 (2017) 356–362, https://doi.org/10.1016/j.colsurfb.2017.07.014.
[8] K.M. Tsoi, S.A. MacParland, X.-Z. Ma, V.N. Spetzler, J. Echeverri, B. Ouyang, S. M. Fadel, E.A. Sykes, N. Goldaracena, J.M. Kaths, et al., Mechanism of hard-nanomaterial clearance by the liver, Nat. Mater. 15 (2016) 1212–1221, https://doi.org/10.1038/nmat4718.
[9] N. Bertrand, J.-C. Leroux, The journey of a drug-carrier in the body: an anatomo-physiological perspective, J. Control. Release 161 (2012) 152–163, https://doi.org/10.1016/j.jconrel.2011.09.098.
[10] A.J. Tavares, W. Poon, Y.-N. Zhang, Q. Dai, R. Besla, D. Ding, B. Ouyang, A. Li, J. Chen, G. Zheng, et al., Effect of removing Kupffer cells on nanoparticle tumor delivery, PNAS 114 (2017) E10871–E10880, https://doi.org/10.1073/pnas.1713390114.
[11] D. Boraschi, P. Italiani, R. Palomba, P. Decuzzi, A. Duschl, B. Fadeel, S. M. Moghimi, Nanoparticles and innate immunity: new perspectives on host defence, Semin. Immunol. 34 (2017) 33–51, https://doi.org/10.1016/j.smim.2017.08.013.
[12] D.E. Owens, N.A. Peppas, Opsonization, biodistribution, and pharmacokinetics of polymeric nanoparticles, Int. J. Pharm. 307 (2006) 93–102, https://doi.org/10.1016/j.ijpharm.2005.10.010.
[13] T.U. Wani, S.N. Raza, N.A. Khan, Nanoparticle opsonization: forces involved and protection by long chain polymers, Polym. Bull. 77 (2020) 3865–3889, https://doi.org/10.1007/s00289-019-02924-7.
[14] J. Lu, X. Gao, S. Wang, Y. He, X. Ma, T. Zhang, X. Liu, Advanced strategies to evade the mononuclear phagocyte system clearance of nanomaterials, Exploration (Beijing, China) 3 (2023) 20220045, https://doi.org/10.1002/EXP.20220045.
[15] S. Panico, S. Capolla, S. Bozzer, G. Toffoli, M. Dal Bo, P. Macor, Biological features of nanoparticles: protein corona formation and interaction with the immune system, Pharmaceutics 14 (2022), https://doi.org/10.3390/pharmaceutics14122605.
[16] G.L. Szeto, E.B. Lavik, Materials design at the interface of nanoparticles and innate immunity, J. Mater. Chem. B 4 (2016) 1610–1618, https://doi.org/10.1039/C5TB01825K.
[17] Da Shi, D. Beasock, A. Fessler, J. Szebeni, J.Y. Ljubimova, K.A. Afonin, M. A. Dobrovolskaia, To PEGylate or not to PEGylate: immunological properties of nanomedicine's most popular component, polyethylene glycol and its alternatives, Adv. Drug Deliv. Rev. 180 (2022) 114079, https://doi.org/10.1016/j.addr.2021.114079.
[18] M. Pannuzzo, S. Esposito, L.-P. Wu, J. Key, S. Aryal, C. Celia, L. Di Marzio, S. M. Moghimi, P. Decuzzi, Overcoming nanoparticle-mediated complement activation by surface PEG pairing, Nano Lett. 20 (2020) 4312–4321, https://doi.org/10.1021/acs.nanolett.0c01011.
[19] J.L. Perry, K.G. Reuter, M.P. Kai, K.P. Herlihy, S.W. Jones, J.C. Luft, M. Napier, J. E. Bear, J.M. DeSimone, PEGylated PRINT nanoparticles: the impact of PEG density on protein binding, macrophage association, biodistribution, and pharmacokinetics, Nano Lett. 12 (2012) 5304–5310, https://doi.org/10.1021/nl302638g.
[20] L. Mi, S. Jiang, Integrated antimicrobial and nonfouling zwitterionic polymers, Angewandte Chemie (International ed. in English) 53 (2014) 1746–1754, https://doi.org/10.1002/anie.201304060.
[21] Z. Han, S. Sarkar, A.M. Smith, Zwitterion and Oligo(ethylene glycol) synergy minimizes nonspecific binding of compact quantum dots, ACS Nano 14 (2020) 3227–3241, https://doi.org/10.1021/acsnano.9b08658.
[22] M. Harijan, M. Singh, Zwitterionic polymers in drug delivery: a review, J. Mol. Recog. JMR 35 (2022) e2944.
[23] X. Zhen, P. Cheng, K. Pu, Recent advances in cell membrane-camouflaged nanoparticles for cancer phototherapy, Small 15 (2019) e1804105, https://doi.org/10.1002/smll.201804105.
[24] I.V. Zelepukin, A.V. Yaremenko, V.O. Shipunova, A.V. Babenyshev, I.V. Balalaeva, P.I. Nikitin, S.M. Deyev, M.P. Nikitin, Nanoparticle-based drug delivery via RBC-hitchhiking for the inhibition of lung metastases growth, Nanoscale 11 (2019) 1636–1646, https://doi.org/10.1039/c8nr07730d.
[25] Y. Qie, H. Yuan, C.A. von Roemeling, Y. Chen, X. Liu, K.D. Shih, J.A. Knight, H. W. Tun, R.E. Wharen, W. Jiang, et al., Surface modification of nanoparticles enables selective evasion of phagocytic clearance by distinct macrophage phenotypes, Sci. Rep. 6 (2016) 26269, https://doi.org/10.1038/srep26269.
[26] P.L. Rodriguez, T. Harada, D.A. Christian, D.A. Pantano, R.K. Tsai, D.E. Discher, Minimal, "self" peptides that inhibit phagocytic clearance and enhance delivery of nanoparticles, Science (New York, N.Y.) 339 (2013) 971–975, https://doi.org/10.1126/science.1229568.
[27] J. Kim, S. Sinha, M. Solomon, E. Perez-Herrero, J. Hsu, Z. Tsinas, S. Muro, Co-coating of receptor-targeted drug nanocarriers with anti-phagocytic moieties enhances specific tissue uptake versus non-specific phagocytic clearance, Biomaterials 147 (2017) 14–25, https://doi.org/10.1016/j.biomaterials.2017.08.045.
[28] T.E. Papp, J. Zeng, H. Shahnawaz, A. Akyianu, L. Breda, A. Yadegari, J. Steward, R. Shi, Q. Li, B.L. Mui, et al., CD47 peptide-cloaked lipid nanoparticles promote cell-specific mRNA delivery, Mol. Ther. 33 (2025) 3195–3208, https://doi.org/10.1016/j.ymthe.2025.03.018.
[29] A. Sawdon, C.-A. Peng, Engineering antiphagocytic biomimetic drug carriers, Ther. Deliv. 4 (2013) 825–839, https://doi.org/10.4155/tde.13.54.
[30] J. Pelt, S. Busatto, M. Ferrari, E.A. Thompson, K. Mody, J. Wolfram, Chloroquine and nanoparticle drug delivery: a promising combination, Pharmacol. Ther. 191 (2018) 43–49, https://doi.org/10.1016/j.pharmthera.2018.06.007.
[31] A. Khalid, S. Persano, H. Shen, Y. Zhao, E. Blanco, M. Ferrari, J. Wolfram, Strategies for improving drug delivery: nanocarriers and microenvironmental priming, Expert Opin. Drug Deliv. 14 (2017) 865–877, https://doi.org/10.1080/17425247.2017.1243527.
[32] Z. Belhadj, B. He, J. Fu, H. Zhang, X. Wang, W. Dai, Q. Zhang, Regulating Interactions between targeted nanocarriers and mononuclear phagocyte system via an esomeprazole-based preconditioning strategy, Int. J. Nanomed. 15 (2020) 6385–6399, https://doi.org/10.2147/IJN.S258054.
[33] J. Wolfram, S. Nizzero, H. Liu, F. Li, G. Zhang, Z. Li, H. Shen, E. Blanco, M. Ferrari, A chloroquine-induced macrophage-preconditioning strategy for improved nanodelivery, Sci. Rep. 7 (2017) 13738, https://doi.org/10.1038/s41598-017-14221-2.
[34] R.T. Proffitt, L.E. Williams, C.A. Presant, G.W. Tin, J.A. Uliana, R.C. Gamble, J. D. Baldeschwieler, Liposomal blockade of the reticuloendothelial system: improved tumor imaging with small unilamellar vesicles, Science (New York, N.Y.) 220 (1983) 502–505, https://doi.org/10.1126/science.6836294.
[35] A.B. Mirkasymov, I.V. Zelepukin, P.I. Nikitin, M.P. Nikitin, S.M. Deyev, In vivo blockade of mononuclear phagocyte system with solid nanoparticles: Efficiency and affecting factors, J. Control. Release 330 (2021) 111–118, https://doi.org/10.1016/j.jconrel.2020.12.004.
[36] N.R.M. Saunders, M.S. Paolini, O.S. Fenton, L. Poul, J. Devalliere, F. Mpambani, A. Darmon, M. Bergère, O. Jibault, M. Germain, et al., A Nanoprimer to improve the systemic delivery of siRNA and mRNA, Nano Lett. 20 (2020) 4264–4269, https://doi.org/10.1021/acs.nanolett.0c00752.
[37] M. Kumar, P. Kulkarni, S. Liu, N. Chemuturi, D.K. Shah, Nanoparticle biodistribution coefficients: a quantitative approach for understanding the tissue distribution of nanoparticles, Adv. Drug Deliv. Rev. 194 (2023) 114708, https://doi.org/10.1016/j.addr.2023.114708.

[38] G.P. Howard, G. Verma, X. Ke, W.M. Thayer, T. Hamerly, V.K. Baxter, J.E. Lee, R. R. Dinglasan, H.-Q. Mao, Critical size limit of biodegradable nanoparticles for enhanced lymph node trafficking and paracortex penetration, Nano Res. 12 (2019) 837–844, https://doi.org/10.1007/s12274-019-2301-3.
[39] S. Kang, S. Ahn, J. Lee, J.Y. Kim, M. Choi, V. Gujrati, H. Kim, J. Kim, E.-C. Shin, S. Jon, Effects of gold nanoparticle-based vaccine size on lymph node delivery and cytotoxic T-lymphocyte responses, J. Control. Release 256 (2017) 56–67, https://doi.org/10.1016/j.jconrel.2017.04.024.
[40] L.M. Kaminskas, C.J.H. Porter, Targeting the lymphatics using dendritic polymers (dendrimers), Adv. Drug Deliv. Rev. 63 (2011) 890–900, https://doi.org/10.1016/j.addr.2011.05.016.
[41] S. Perazzolo, D.D. Shen, R.J.Y. Ho, Physiologically based pharmacokinetic modeling of 3 hiv drugs in combination and the role of lymphatic system after subcutaneous dosing. Part 2: model for the drug-combination nanoparticles, J. Pharm. Sci. 111 (2022) 825–837, https://doi.org/10.1016/j.xphs.2021.10.009.
[42] T. Stack, Y. Liu, M. Frey, S. Bobbala, M. Vincent, E. Scott, Enhancing subcutaneous injection and target tissue accumulation of nanoparticles via co-administration with macropinocytosis inhibitory nanoparticles (MiNP), Nanoscale Horiz. 6 (2021) 393–400, https://doi.org/10.1039/d0nh00679c.
[43] K. Schorr, S. Beck, O. Zimmer, F. Baumann, M. Keller, R. Witzgall, A. Goepferich, The quantity of ligand-receptor interactions between nanoparticles and target cells, Nanoscale Horiz. 10 (2025) 803–823, https://doi.org/10.1039/d4nh00645c.
[44] D. Fleischmann, S. Maslanka Figueroa, S. Beck, K. Abstiens, R. Witzgall, F. Schweda, P. Tauber, A. Goepferich, Adenovirus-mimetic nanoparticles: sequential ligand-receptor interplay as a universal tool for enhanced in vitro/in vivo cell identification, ACS Appl. Mater. Interfaces 12 (2020) 34689–34702, https://doi.org/10.1021/acsami.0c10057.
[45] K. Abstiens, M. Gregoritza, A.M. Goepferich, Ligand density and linker length are critical factors for multivalent nanoparticle-receptor interactions, ACS Appl. Mater. Interfaces 11 (2019) 1311–1320, https://doi.org/10.1021/acsami.8b18843.
[46] H. Yang, Y.-Z. Chen, Y. Zhang, X. Wang, X. Zhao, J.I. Godfroy, Q. Liang, M. Zhang, T. Zhang, Q. Yuan, et al., A lysine-rich motif in the phosphatidylserine receptor PSR-1 mediates recognition and removal of apoptotic cells, Nat. Commun. 6 (2015) 5717, https://doi.org/10.1038/ncomms6717.
[47] M.K. Callahan, P.M. Popernack, S. Tsutsui, L. Truong, R.A. Schlegel, A. J. Henderson, Phosphatidylserine on HIV envelope is a cofactor for infection of monocytic cells, J. Immunol. (Baltimore, Md.: 1950) 2003 (170) (2003) 4840–4845, https://doi.org/10.4049/jimmunol.170.9.4840.
[48] Z. Xu, J. Li, N. Yan, X. Liu, Y. Deng, Y. Song, Phosphatidylserine and/or sialic acid modified liposomes increase uptake by tumor-associated macrophages and enhance the anti-tumor effect, AAPS PharmSciTech 25 (2024) 125, https://doi.org/10.1208/s12249-024-02837-3.
[49] S. Maslanka Figueroa, D. Fleischmann, S. Beck, A. Goepferich, the effect of ligand mobility on the cellular interaction of multivalent nanoparticles, Macromol. Biosci. 20 (2020) e1900427, https://doi.org/10.1002/mabi.201900427.
[50] A. Kathrin, G. Achim, Interaction of functionalized PEG-PLA/PLGA nanoparticles with serum proteins and impact on nanoparticle stability and cell toxicity, Front. Bioeng. Biotechnol. 4 (2016), https://doi.org/10.3389/conf.FBIOE.2016.01.02161.
[51] M. Walter, H. Weißbach, F. Gembardt, S. Halder, K. Schorr, D. Fleischmann, V. Todorov, C. Hugo, A. Goepferich, Long-term residence and efficacy of adenovirus-mimetic nanoparticles in renal target tissue, J. Drug Target. 32 (2024) 1320–1332, https://doi.org/10.1080/1061186X.2024.2390628.
[52] J. Groner, M. Tognazzi, M. Walter, D. Fleischmann, R. Mietzner, C.E. Ziegler, A. M. Goepferich, M. Breunig, Encapsulation of pioglitazone into polymer-nanoparticles for potential treatment of atherosclerotic diseases, ACS Appl. Bio Mater. 6 (2023) 2111–2121, https://doi.org/10.1021/acsabm.2c01001.
[53] M. Walter, M. Bresinsky, O. Zimmer, S. Pockes, A. Goepferich, Conditional cell-penetrating peptide exposure as selective nanoparticle uptake signal, ACS Appl. Mater. Interfaces 16 (2024) 37734–37747, https://doi.org/10.1021/acsami.4c07821.
[54] A.K. Parthipan, N. Gupta, K. Pandey, B. Sharma, J. Jacob, S. Saha, One-step fabrication of bicompartmental microparticles as a dual drug delivery system for Parkinson's disease management, J. Mater. Sci. 54 (2019) 730–744, https://doi.org/10.1007/s10853-018-2819-x.
[55] M. Bohley, A. Haunberger, A.M. Goepferich, Intracellular availability of poorly soluble drugs from lipid nanocapsules, Eur. J. Pharm. Biopharm. 139 (2019) 23–32, https://doi.org/10.1016/j.ejpb.2019.03.007.
[56] M. Bohley, A.E. Dillinger, F. Schweda, A. Ohlmann, B.M. Braunger, E.R. Tamm, A. Goepferich, A single intravenous injection of cyclosporin A-loaded lipid nanocapsules prevents retinopathy of prematurity, Sci. Adv. 8 (2022) eabo6638, https://doi.org/10.1126/sciadv.abo6638.
[57] Empfehlung zur Substanzapplikation bei Versuchstieren, 2017.
[58] X.-J. Du, J.-L. Wang, W.-W. Liu, J.-X. Yang, C.-Y. Sun, R. Sun, H.-J. Li, S. Shen, Y.-L. Luo, X.-D. Ye, et al., Regulating the surface poly(ethylene glycol) density of polymeric nanoparticles and evaluating its role in drug delivery in vivo, Biomaterials 69 (2015) 1–11, https://doi.org/10.1016/j.biomaterials.2015.07.048.
[59] O. Zimmer, A. Goepferich, How clathrin-coated pits control nanoparticle avidity for cells, Nanoscale Horiz. 8 (2023) 256–269, https://doi.org/10.1039/d2nh00543c.
[60] S.T. Reddy, A.J. van der Vlies, E. Simeoni, V. Angeli, G.J. Randolph, C.P. O'Neil, L. K. Lee, M.A. Swartz, J.A. Hubbell, Exploiting lymphatic transport and complement activation in nanoparticle vaccines, Nat. Biotechnol. 25 (2007) 1159–1164, https://doi.org/10.1038/nbt1332.
[61] B. Ouyang, W. Poon, Y.-N. Zhang, Z.P. Lin, B.R. Kingston, A.J. Tavares, Y. Zhang, J. Chen, M.S. Valic, A.M. Syed, et al., The dose threshold for nanoparticle tumour delivery, Nat. Mater. 19 (2020) 1362–1371, https://doi.org/10.1038/s41563-020-0755-z.
[62] A.B. Mirkasymov, I.V. Zelepukin, I.N. Ivanov, I.B. Belyaev, D.Sh. Dzhalilova, D. B. Trushina, A.V. Yaremenko, Yu.V. Ivanov, M. Nikitin, P.I. Nikitin, et al., Macrophage blockade using nature-inspired ferrihydrite for enhanced nanoparticle delivery to tumor, Int. J. Pharm. 621 (2022) 121795, https://doi.org/10.1016/j.ijpharm.2022.121795.
[63] Y.-N. Zhang, W. Poon, A.J. Tavares, I.D. McGilvray, W.C. Chan, Nanoparticle–liver interactions: cellular uptake and hepatobiliary elimination, J. Control. Release 240 (2016) 332–348, https://doi.org/10.1016/j.jconrel.2016.01.020.
[64] F. Montanari, M. Lu, S. Marcus, A. Saran, A. Malankar, A. Mazumder, A phase II trial of chloroquine in combination with bortezomib and cyclophosphamide in patients with relapsed and refractory multiple myeloma, Blood 124 (2014) 5775, https://doi.org/10.1182/blood.V124.21.5775.5775.
[65] A. Chow, B.D. Brown, M. Merad, Studying the mononuclear phagocyte system in the molecular age, Nat. Rev. Immunol. 11 (2011) 788–798, https://doi.org/10.1038/nri3087.
[66] Y. Tang, X. Wang, J. Li, Y. Nie, G. Liao, Y. Yu, C. Li, Overcoming the reticuloendothelial system barrier to drug delivery with a "Don't-Eat-Us" strategy, ACS Nano 13 (2019) 13015–13026, https://doi.org/10.1021/acsnano.9b05679.
[67] K. Morizono, I.S.Y. Chen, Role of phosphatidylserine receptors in enveloped virus infection, J. Virol. 88 (2014) 4275–4290, https://doi.org/10.1128/JVI.03287-13.
[68] M. Yeom, D.-H. Hahm, B.-J. Sur, J.-J. Han, H.-J. Lee, H.-I. Yang, K.S. Kim, Phosphatidylserine inhibits inflammatory responses in interleukin-1β–stimulated fibroblast-like synoviocytes and alleviates carrageenan-induced arthritis in rat, Nutr. Res. 33 (2013) 242–250, https://doi.org/10.1016/j.nutres.2013.01.006.
[69] M.A. Shetab Boushehri, D. Dietrich, A. Lamprecht, Nanotechnology as a platform for the development of injectable parenteral formulations: a comprehensive review of the know-hows and state of the art, Pharmaceutics 12 (2020), https://doi.org/10.3390/pharmaceutics12060510.
[70] Z. Wan, L. Zhao, F. Lu, X. Gao, Y. Dong, Y. Zhao, M. Wei, G. Yang, C. Xing, L. Liu, Mononuclear phagocyte system blockade improves therapeutic exosome delivery to the myocardium, Theranostics 10 (2020) 218–230, https://doi.org/10.7150/thno.38198.
[71] J. Hao, T. Han, M. Wang, Q. Zhuang, X. Wang, J. Liu, Y. Wang, H. Tang, Temporary suppression the sequestrated function of host macrophages for better nanoparticles tumor delivery, Drug Deliv. 25 (2018) 1289–1301, https://doi.org/10.1080/10717544.2018.1474965.
[72] T. Miller, S. Breyer, G. van Colen, W. Mier, U. Haberkorn, S. Geissler, S. Voss, M. Weigandt, A. Goepferich, Premature drug release of polymeric micelles and its effects on tumor targeting, Int. J. Pharm. 445 (2013) 117–124, https://doi.org/10.1016/j.ijpharm.2013.01.059.
[73] K. Elbrink, S. van Hees, R. Chamanza, D. Roelant, T. Loomans, R. Holm, F. Kiekens, Application of solid lipid nanoparticles as a long-term drug delivery platform for intramuscular and subcutaneous administration: In vitro and in vivo evaluation, Eur. J. Pharm. Biopharm. 163 (2021) 158–170, https://doi.org/10.1016/j.ejpb.2021.04.004.
[74] S. Zhu, X. Li, D.S.P. Lansakara-P, A. Kumar, Z. Cui, A nanoparticle depot formulation of 4-(N)-stearoyl gemcitabine shows a strong anti-tumour activity, J. Pharm. Pharmacol. 65 (2013) 236–242, https://doi.org/10.1111/j.2042-7158.2012.01599.x.
[75] R. Pandey, G.K. Khuller, Subcutaneous nanoparticle-based antitubercular chemotherapy in an experimental model, J. Antimicrob. Chemother. 54 (2004) 266–268, https://doi.org/10.1093/jac/dkh260.
[76] R.R. Arvizo, O.R. Miranda, D.F. Moyano, C.A. Walden, K. Giri, R. Bhattacharya, J. D. Robertson, V.M. Rotello, J.M. Reid, P. Mukherjee, Modulating pharmacokinetics, tumor uptake and biodistribution by engineered nanoparticles, PLoS One 6 (2011) e24374, https://doi.org/10.1371/journal.pone.0024374.
[77] K. Schorr, X. Chen, T. Sasaki, A.P. Arias-Loza, J. Lang, T. Higuchi, A. Goepferich, Rethinking thin-layer chromatography for screening technetium-99m radiolabeled polymer nanoparticles, ACS Pharmacol. Transl. Sci. 7 (2024) 2604–2611, https://doi.org/10.1021/acsptsci.4c00383.
[78] M. Bohley, A. Haunberger, A.M. Goepferich, Intracellular availability of poorly soluble drugs from lipid nanocapsules, European J. Pharm. Biopharm.: Official Journal of Arbeitsgemeinschaft Fur Pharmazeutische Verfahrenstechnik E.v 139 (2019) 23–32, https://doi.org/10.1016/j.ejpb.2019.03.007.
[79] T.A. Miranda, P.H.R. Silva, G.A. Pianetti, I.C. César, Simultaneous quantitation of chloroquine and primaquine by UPLC-DAD and comparison with a HPLC-DAD method, Malar. J. 14 (2015) 29, https://doi.org/10.1186/s12936-015-0570-1.